DEVELOPMENTS IN TRANSONIC STEADY AND UNSTEADY FLOW THEORY

John R. Spreiter
Stanford University
Stanford, California

and

Stephen S. Stahara
Nielsen Engineering & Research, Inc.
Mountain View, California

Abstract

Great strides have been made in recent years in the analysis of transonic flows past wings and bodies, and the initial extensions to wing-body combinations, helicopter rotors, and internal flow through rotating turbomachinery have been announced. Although the methods are too numerous and diverse to permit detailed description, the salient features and results of the more significant are reviwed.

I. Introduction

With the propsect of efficient transonic flight afforded by the development of supercritical airfoils providing the motivation, with the results (1-5) of a previous era extending from about 15 to 25 years ago providing the foundation, and with an enhanced computational capability providing the means, enormous progress in transonic flow analysis is currently being made. During this decade, several new methods particularly adapted for use with advanced computers have been developed to calculate flows about increasingly complex aerodynamic configurations. These techniques are not limited to the small disturbance theory that formed the basis for most of the earlier work, but apply also to (a) the complete potential equation for irrotational flow, (b) the Euler equations for general inviscid flow, and (c) even the Navier-Stokes equations for viscous flow. Some of the methods, such as the numerical time-dependent procedures, have been applied to all levels of description. Others, as the hodograph, are restricted to two-dimensional steady flow governed by either the complete potential equation or its small disturbance counterpart. Still others, as the integral equation method, have broader potentialities, but are presently developed primarily for the small disturbance equation. As might be expected, most methods have been applied to the small disturbance formulation and fewest to the Navier-Stokes equations. Under favorable circumstances, the various methods yield similar results, with the effects of viscosity being confined to limited regions, so that the results of the small disturbance theory agree with those of the more accurate theories. Some of the differences, moreover, stem directly from differences in computational details such as mesh size, order of accuracy of the difference algorithm, etc., and could be reduced at the expense of greater computing time or with the development of more effective algorithms.

Because the volume of material is so large, and reference can be made to several excellent reviews (6-11) as well as the original papers, our approach here is to provide a broad overview by combining brief accounts of the theoretical basis of the various methods followed by a presentation and discussion of significant results, usually obtained by more than one method. We start with two-dimensional flows, for which the number and variety of methods is greatest, and with the Navier-Stokes representation so that the initial results presented will provide a standard with which the following approximate theories can be judged. Three-dimensional flows are discussed subsequently.

II. Two-Dimensional Flow

Although the majority of analysis has been directed toward an inviscid level of approximation, transonic flows are often highly influenced by viscous phenomena, particularly shock-induced boundary-layer separation. The most complete analysis of such a flow is that of Diewert(12,13) who employs the finite volume method to solve the time-dependent, Reynolds-averaged Navier-Stokes equations which, written in integral form, are

$$\frac{\partial}{\partial t}\int_{vol}\begin{Bmatrix}\rho\\ \rho U\\ \rho W\\ E\end{Bmatrix} d\,vol + \int_S \begin{Bmatrix}\rho\underset{\sim}{q}\\ \rho U\underset{\sim}{q} + \bar{\underset{\sim}{\tau}}\cdot\hat{i}_x\\ \rho V\underset{\sim}{q} + \bar{\underset{\sim}{\tau}}\cdot\hat{i}_y\\ E\underset{\sim}{q} + \bar{\underset{\sim}{\tau}}\cdot\underset{\sim}{q} - \kappa\underset{\sim}{\nabla}T\end{Bmatrix}\cdot\hat{n}\, dS = 0 \qquad (1)$$

where

$$\underset{\sim}{q} = \hat{i}_x U + \hat{i}_z W,$$

$$\bar{\underset{\sim}{\tau}} = \hat{i}_x\hat{i}_x\sigma_x + \hat{i}_x\hat{i}_z\tau_{xz} + \hat{i}_z\hat{i}_x\tau_{zx} + \hat{i}_z\hat{i}_z\sigma_{zz}$$

in which ρ is density, U and W are velocity components and $\hat{i}_x$ and $\hat{i}_z$ are unit vectors parallel to the x and z axes, $E = e + (U^2 + V^2)/2$ is total energy per unit volume, κ is thermal conductivity, $\underset{\sim}{\nabla}T$ is temperature gradient, σ and τ are normal and shear stresses, and $\hat{n}$ is a unit normal vector. In addition to ordinary viscous stresses in τ, Diewert also includes turbulent Reynolds stresses estimated using four different algebraic eddy viscosity models. If the viscous and Reynolds stresses are disregard, Eq. (1) reduces to the integral form of the Euler equations for inviscid flow,

$$\frac{\partial}{\partial t}\int_{vol}\begin{Bmatrix}\rho\\ \rho U\\ \rho W\\ E\end{Bmatrix} d\,vol + \int_S \begin{Bmatrix}\rho\underset{\sim}{q}\\ \rho U\\ \rho W\\ E\end{Bmatrix}\underset{\sim}{q}\cdot\hat{n}\, dS + \int_S \begin{Bmatrix}0\\ p\,\hat{n}\\ p\,\hat{n}\\ p\,\underset{\sim}{q}\cdot\hat{n}\end{Bmatrix} dS = 0 \qquad (2)$$

The integral forms are appropriate for the finite volume method used by Diewert for viscous flow and also by Rizzi(14) for inviscid flow; but other methods are usually derived from the

corresponding differential equations. The Euler equations, for example, are as follows when written in conservation form to include the shock relations directly

$$\frac{\partial}{\partial t}\begin{Bmatrix}\rho\\ \rho U\\ \rho W\\ E\end{Bmatrix}+\frac{\partial}{\partial x}\begin{Bmatrix}\rho U\\ \rho U^2+p\\ \rho UW\\ U(E+p)\end{Bmatrix}+\frac{\partial}{\partial z}\begin{Bmatrix}\rho W\\ \rho UW\\ \rho W^2+p\\ W(E+p)\end{Bmatrix}=0 \qquad (3)$$

Since these equations are difficult to solve, they are often approximated by assuming the flow to be isentropic. This is correct without approximation for flows which are continuous, i.e., shock-free, and a good approximation for flows with shock waves if they are not too strong. Under these circumstances,

$$(p/p_\infty)/(\rho/\rho_\infty)^\gamma = \exp\,[(s-s_\infty)/c_v] \qquad (4)$$

where $\gamma = c_p/c_v$ is the ratio of specific heats at constant volume and pressure, s is entropy, and subscript ∞ refers to free-stream conditions. Then Eq. (3) reduces to

$$\frac{\partial}{\partial t}\begin{Bmatrix}\rho\\ \rho U\\ \rho W\end{Bmatrix}+\frac{\partial}{\partial x}\begin{Bmatrix}\rho U\\ \rho U^2+p_o(\rho/\rho_o)^\gamma\\ \rho UW\end{Bmatrix}+\frac{\partial}{\partial z}\begin{Bmatrix}\rho W\\ \rho UW\\ \rho W^2+p_o(\rho/\rho_o)^\gamma\end{Bmatrix}=0 \qquad (5)$$

Magnus and Yoshihara[15] have introduced time-dependent numerical methods to transonic analysis by solving these equations.

A related assumption, which is also exact for shock-free flow and a good approximation if the shock waves are not too strong, is that the flow is irrotational. There then exists a velocity potential Φ related to the velocity by $\underset{\sim}{q} = \underset{\sim}{\nabla}\Phi$ that satisfies

$$(a^2-\Phi_x^2)\Phi_{xx}-2\Phi_x\Phi_z\Phi_{xz}+(a^2-\Phi_z^2)\Phi_{zz}-\Phi_{tt}-2\Phi_x\Phi_{xt}-2\Phi_z\Phi_{zt}=0 \qquad (6)$$

where $a=[a_o^2-(\gamma-1)q^2/2]^{1/2}$ is the local speed of sound, and a_o is the stagnation speed of sound. When applied to steady flow so that the time derivatives vanish, Eq. (6) is of elliptic type where the local Mach number $M = |\underset{\sim}{q}|/a < 1$, and hyperbolic type where $M = |\underset{\sim}{q}|/a > 1$. Both the hodograph and finite difference relaxation methods have been used extensively to solve this equation.

Most transonic analysis both past and present has, however, been based on a small disturbance approximation to Eq. (6). For flow with free-stream velocity $\underset{\sim}{q}_\infty = \hat{i}_x U_\infty$ past a thin airfoil aligned approximately with the x axis, a perturbation velocity potential $\phi = \Phi - U_\infty x$ can be introduced and shown to satisfy

$$(1-M_\infty^2-k\phi_x)\phi_{xx}+\phi_{zz}-\frac{2M_\infty^2}{U_\infty}\phi_{xt}-\frac{M_\infty^2}{U_\infty}\phi_{tt}=0 \qquad (7)$$

For $M_\infty = U_\infty/a_\infty \neq 1$, a number of alternatives exist for k, but the widely used expression $k = (\gamma+1)M_\infty^2/U_\infty$ provides a good all-around compromise.

Equations (1) through (7) must be supplemented by boundary conditions and other relations to specify both a mathematical problem corresponding to a physical application and a unique solution. Boundary conditions must describe conditions at infinity and at the airfoil surface. With Eq. (1), the velocity must satisfy the no-slip condition at the airfoil surface; whereas only the normal component must match that of the airfoil surface with Eqs. (2) through (7). With Eq. (7), it is customary to linearize the boundary condition and transfer it to the x axis. Thus,

$$(\phi_z)_{z=0} = U_\infty\left(\frac{\partial Z}{\partial x}+\frac{1}{U_\infty}\frac{\partial Z}{\partial t}\right) \qquad (8)$$

for an airfoil having ordinates $Z(x,t)$. Similarly, the exact Bernoulli equation is used with Eq. (6), whereas an approximation

$$C_p = \frac{p-p_\infty}{\frac{\rho_\infty}{2}q_\infty^2} = -\frac{2}{U_\infty}\left(\phi_x+\frac{1}{U_\infty}\phi_t\right) \qquad (9)$$

is normally used with Eq. (7). Equations (1) through (5) do not need supplementary relations for shock waves, but Eqs. (6) and (7) do. To complete the specification for a lifting airfoil, it is also necessary to impose the Kutta condition or some counterpart.

Of the many methods for solving steady transonic flow problems, the hodograph method is unique in that it depends on a transformation that linearizes the governing equation without approximation by interchanging the dependent and independent variables. In this way, the steady-state form of Eq. (6) transforms to

$$(a^2-U^2)\phi_{UU}-2UW\,\phi_{UW}+(a^2-W^2)\phi_{WW}=0 \qquad (10)$$

and its small disturbance counterpart, Eq. (7), to

$$(1-M_\infty^2-ku)\phi_{ww}+\phi_{uu}=0 \qquad (11)$$

in which ϕ is the Legendre potential related to the coordinates by $\phi_u = x$ and $\phi_w = z$. The Jacobian of the transformation, $J = u_x^2(M_\infty^2-1+ku)-u_z^2$ in the case of Eq. (11), cannot vanish where the flow is subsonic, but may vanish where it is supersonic, thereby signifying an inconvenient multiple mapping in the hodograph plane of a single point in the physical plane. As a result, use of this method is usually confined to the subsonic region and a limited part of the supersonic region unless the latter is small as at slightly supercritical Mach numbers. The remainder of the solution is calculated by another method, such as characteristics or finite differences. The hodograph method was used extensively in the early development of transonic flow theory[2,4], but difficulties in imposing boundary conditions for an airfoil of specified shape restricted its usefulness. It has come into a new era of significance in the design of shock-free airfoils for which it is particularly well suited.

Two methods of solving the hodograph equations are currently predominant. That of Nieuwland[16], Takahashi[17], and Boerstoel[18] relies on function theory and integral transforms; that of Bauer, Garabedian, and Korn[19,20] is based on analytical continuation into the complex domain so that the solution can be obtained by solving initial value problems. Both methods culminate with extensive numerical computations.

The first method to be developed for shocked transonic flow that depends intrinsically on the modern electronic computer is the time-dependent method of Magnus and Yoshihara[15,21,22]. It applies a modified Lax-Wendroff difference scheme to Eq. (5) to compute from a knowledge of ρ, U, and W at one time new values for a slightly later time. Repetitive application provides a time history of the development of the flow from an assumed initial state. Solutions for steady flow are obtained by imposing steady boundary conditions and carrying the calculations sufficiently forward in time for the transients to disappear, characteristically a costly process.

Relaxation methods were used in the early transonic studies of Emmons[23] in physical variables and Vincenti and Wagoner[24,25] in hodograph variables, but modern applications derive directly from Murman and Cole[26] who introduced the use of different difference expressions in the subsonic and supersonic regions in conformity with the respective domains of influence. The procedure was initially applied to Eq. (10) in which ϕ_{zz} is approximated by centered differences; and ϕ_x and ϕ_{xx} are represented by centered differences in regions of subsonic flow and by one-sided upwind differences in regions of supersonic flow. The resulting large set of algebraic equations was solved numerically using a successive line overrelaxation (SLOR) procedure.

It was soon recognized that the use of only two types of operators for ϕ_x and ϕ_{xx} was insufficient since difficulties arose at the sonic line and shock wave where transitions between the two forms had to be made. The problem was resolved by introducing a sonic finite difference operator corresponding to the centered-difference expression for ϕ_{zz} and a shock operator corresponding to the sum of the subsonic and supersonic operators. The latter when applied to the steady-state form of Eq. (7) rewritten in conservation form

$$[1 - M_\infty^2 - (k/2)\phi_x^2]_x + (\phi_y)_y = 0 \qquad (12)$$

results in substantial improvement of the calculated changes across a shock wave[27]. Presently, two types of differencing procedures are widely used with regard to the small disturbance equation. To distinguish them, those employing the shock point operator (SPO), which assures conservation of mass at shock points, are designated FCR (fully conservative relaxation); while those which do not employ the SPO are termed NCR (not fully conservative relaxation). Further complications arise when the method is applied to the complete potential Eq. (6) specialized to steady flow. The centerline of the Mach forecone region of dependence in supersonic flow is no longer parallel to the x axis, but is in the local direction of the streamlines. The calculations fail to converge if the differencing is done in the same way as in the small disturbance theory since the region of dependence of the differencing scheme does not always include that of the differential equation. However, Jameson[28] showed that convergence could be achieved if the finite difference elements were rotated to allow for the change in direction.

Improvements have also been made in devising more efficient algorithms for solving the large set of algebraic equations provided by the finite difference procedure. The SLOR method employed originally has been supplemented by more efficient procedures[6,8,9,10,29,30], and further advances exploiting steadily improving computer capabilities are to be anticipated.

The integral equation method, stemming from Oswatitsch[31] and Spreiter and Alksne[32], was the first method capable of providing results with embedded shock waves for supercritical flows. In this method, Green's theorem is used to transform the steady-state form of Eq. (7) into a nonlinear integral equation

$$\bar{u} = \bar{u}_L + \nu\bar{u}^2 - \frac{1}{2\pi}\iint \frac{\bar{u}^2}{2}\,\frac{(\bar{x}-\bar{\xi})^2 - (\bar{z}-\bar{\zeta})^2}{[(\bar{x}-\bar{\xi})^2 + (\bar{z}-\bar{\zeta})^2]^2}\,d\bar{\xi}\,d\bar{\zeta} \qquad (13)$$

where $\bar{x} = x$, $\bar{z} = (1 - M_\infty^2)^{1/2} z$, $\bar{u} = u/u_{cr} = ku/(1 - M_\infty^2)$, and u_L represents the solution of Eq. (7) with the nonlinear and time-derivative terms omitted. Originally, the singularity at the field point where $\bar{u}$ is to be evaluated was enclosed by an infinitesimal rectangle having a ratio λ of height to width of infinity, in which case $\nu = 1/2$. Nixon and Hancock[33] have subsequently obtained $\nu = 1/4$ by enclosing the same point by an infinitesimal circle. Ogana and Spreiter[34] have investigated this matter further by enclosing the field point in an infintesimal rectangle of arbitrary λ, for which $\nu = (1/\pi)$ arctan λ. This accounts for the earlier results since $\nu = 1/2$ when $\lambda = \infty$, and $\nu = 1/4$ when $\lambda = 1$. These differences are somewhat illusory, however, since the doublet integral is semi-convergent and its value depends on λ in such a way that the sum of the last two terms of Eq. (13) is independent of the shape of the contour.

Solutions of Eq. (13) were sought initially by introduction of a velocity profile f of the form $\bar{u}(\bar{x},\bar{z}) = \bar{u}(\bar{x},0)f(\bar{x},\bar{z},\bar{u}_{\bar{z}=0},Z)$ so that the double integral could be approximated by a single integral and solutions could be obtained with a modest amount of hand computation[32,35]. Although this method has substantial merit[36], the trend[33,37] is to direct numerical solution. Nixon and Hancock [33] have shown, in addition, that a notable improvement for the vicinity of the leading edge may be achieved by using a modified $\bar{u}_L$ obtained by replacing the boundary condition of Eq. (8) with

$$(\phi_z)_{z=Z} = (U_\infty + \phi_x)_{z=Z}\,\frac{dZ}{dx} \qquad (14)$$

In addition to the above methods that may be refined systematically to provide an essentially exact solution within the framework of small disturbance theory, there are several approximate methods that can provide accurate results, often

very simply. Principal among these are the local linearization[38,39] and the parametric differentiation[40] methods Since they are not in such an active stage of development, no general description will be provided; although their results will be displayed for comparison.

We turn now to the results provided by all of the methods discussed. Figure 1 presents pressure distributions for an 18-percent thick circular-arc airfoil as measured[41], and as calculated by Diewert[12,13] for both inviscid and viscous flow

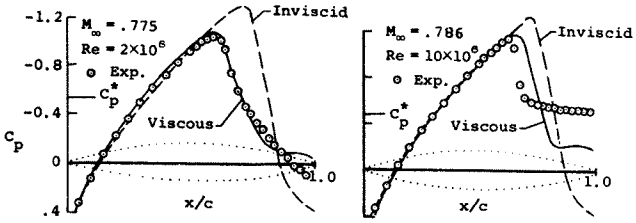

Fig. 1.- Pressure distributions for thick circular-arc airfoil.

by application of the finite volume method to Eq. (1). The inviscid solution agrees well with experiment over the forward half of the airfoil, but is inaccurate in predicting shock strength and location, and the pressure level near the trailing edge. When the aft pressure recovery is strong, as for Reynolds number, Re = 2×10^6, the viscous solution agrees well with experiment. When the aft pressure recovery is weak, the theoretical results disagree, probably because of inadequate turbulent modeling in the separated region. At the present time, these are the most complete comparisons between viscous theory and experiment; the differences should be remembered in evaluating subsequent comparisons between inviscid theory and experiment.

Figure 2 presents a comparison of exact and approximate solutions for steady inviscid shock-free transonic flow past two different supercritical airfoils[10]. It shows that results obtained

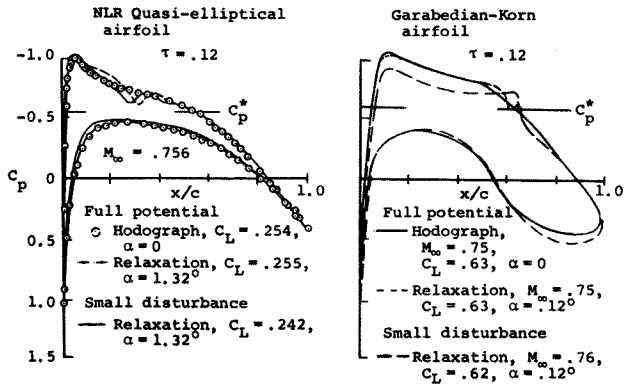

Fig. 2.- Theoretical shock-free pressure distributions for two supercritical airfoils.

by application of finite difference relaxation methods[42,43] to the complete potential Eq. (6), and the hodograph method[43,44] to its counterpart Eq. (10), are virtually identical; and, furthermore, that the transonic small disturbance Eq. (7)[45] can provide results of outstanding accuracy, a conclusion long evident from early studies[3].

Figure 3 from Ballhaus[9] shows pressure distributions for transonic flow with embedded shock wave for an NACA 64A410 airfoil calculated by application

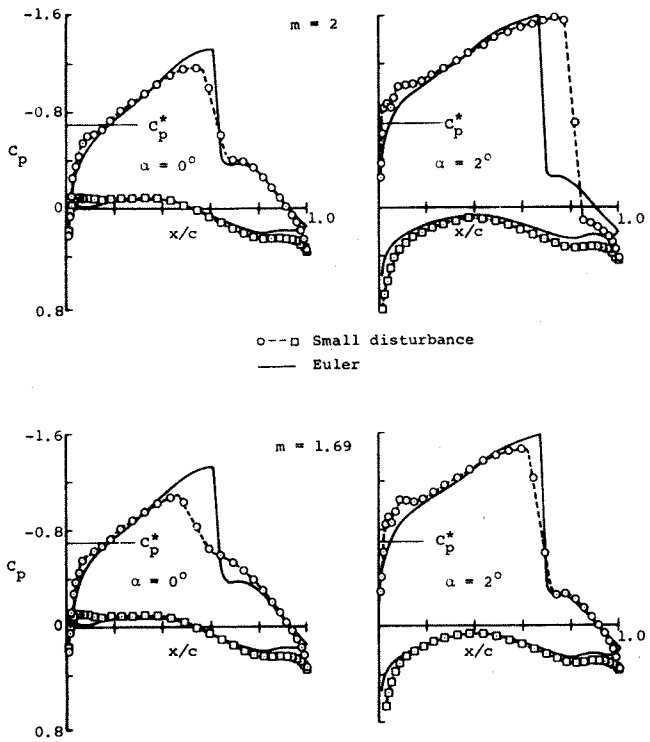

Fig. 3.- Exact and approximate transonic pressure distributions for an NACA 64A410 airfoil at two angles of attack, M_∞ = 0.72.

of the time-dependent method[15,21,22] to the Euler Eqs. (5) for isentropic flow and of the finite difference relaxation method to the small disturbance Eq. (7). Two versions of the latter are shown distinguished by the value of m in $k = M_\infty^m(\gamma+1)/U_\infty$. The upper plots are for m = 2, in wide use for many years[46]. To improve accuracy without complication Krupp[47] has proposed several other values for m, each of which has certain desirable properties such as the accuracy of the approximation for the shock jumps or the critical pressure coefficient, C_p^*. Among these values is m = 1.69 used in the lower plots of Fig. 3. The results illustrate the dilemma encountered in such efforts. The results for m = 1.69 are superior for angle of attack, α = 0, but those for m = 2 are better for α = 2°. To us, it seems preferable to use m = 2 for most applications, reserving other values for restricted classes of applications that emphasize a particular feature of the flow that can be better represented by another value for m.

As noted above, significant differences occur for the vicinity of a shock wave depending on whether the finite differencing is done with the FCR or NCR procedures. These are illustrated in Fig. 4 for a nonlifting 6-percent thick circular-arc airfoil at two different values for M_∞[27].

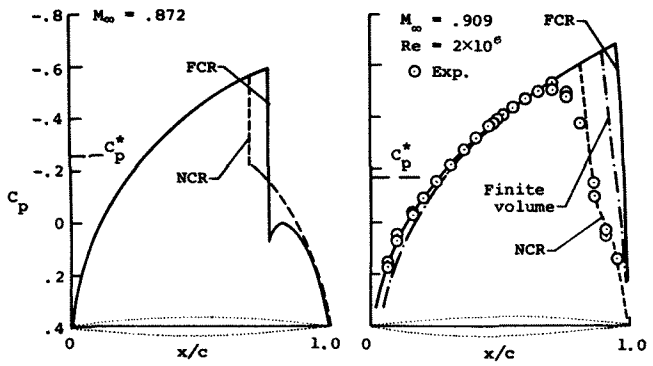

Fig. 4.- Supercritical pressure distributions for a thin circular-arc airfoil indicated by the FCR and NCR solutions of the transonic small disturbance equations, by the finite volume solution of the Euler equations, and by experiment.

Away from the shock wave, the results are in agreement, but near the shock wave they are quite different. In particular, the NCR shock pressure jump does not approach the theoretical normal shock jump; whereas the FCR solution shows not only that the correct condition is attained but that the shock is followed by a well-defined reexpansion, as is proper. The FCR solution also indicates a more downstream location for the shock wave than the NCR solution. Superposed on the results for $M_\infty = 0.909$ are experimental data[48] and a finite volume solution[14] of the Euler Eqs. (2). This comparison confirms that the FCR shock location agrees better with the exact inviscid location than the NCR locations; although the latter agree better with experiment. This paradox can be resolved by reference to Fig. 1 in which it is illustrated how viscous effects lead to a more upstream location of an embedded shock than indicated by inviscid theory. In addition to the differences in the surface pressures illustrated in Fig. 4, Newman and South[49] have shown that the streamlines downstream of the shock are displaced outward substantially and erroneously by the NCR method because of spurious mass addition at the shock. The FCR method avoids this deficiency by satisfying mass conservation everywhere.

Analogous results for the same airfoil in a slightly supersonic stream with $M_\infty = 1.15$ are shown in Fig. 5[10,27]. The calculations were performed using the two relaxation methods and also a finite-difference solution of the Euler Eqs.(5) by

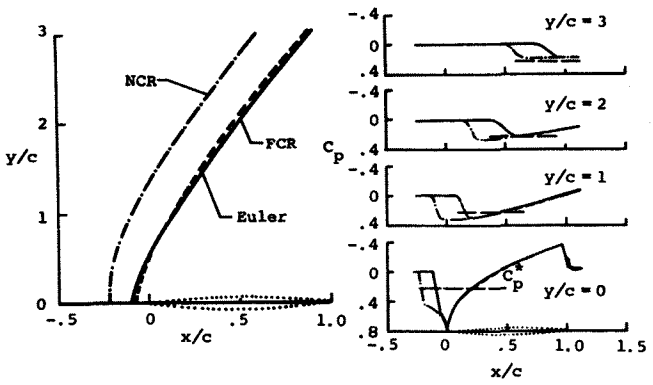

Fig. 5.- Pressure distributions and bow wave locations for a thin circular-arc airfoil indicated by FCR and NCR solutions of the transonic small disturbance equations, and an Euler solution.

a time-dependent method[50], which is fully conservative. All three methods indicate essentially the same pressure distribution on the airfoil, but the NCR method again indicates a location for the shock wave, this time detached, that is too far forward.

Although the integral equation method has been partially eclipsed by the hodograph and relaxation methods, recent reevaluations[33,36,37] indicate that it has considerable merit. Figure 6 shows pressure distributions for a 6-percent thick

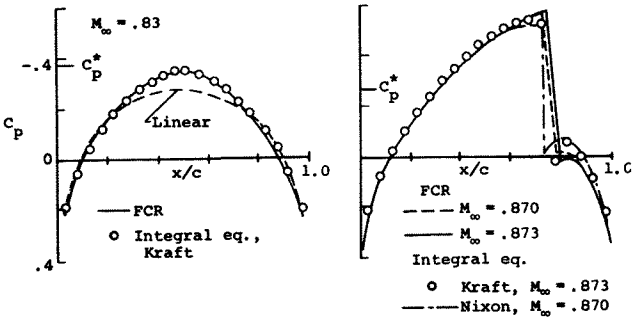

Fig. 6.- Pressure distributions for a 6-percent thick circular-arc airfoil indicated by integral equation and FCR solutions of the transonic small disturbance equation.

circular-arc airfoil calculated using two versions of the integral equation method and the small disturbance FCR finite difference method. The results of Kraft[36] have been determined using a velocity profile to reduce the doublet integral to a single integral and iterating in the manner of Spreiter and Alksne[32]. Those of Nixon[51] have been calculated using his extended integral equation method in which the doublet integral is evaluated by dividing the region of integration into a number of streamwise strips across which interpolation functions are used to express values for the integrand in terms of values along the strip edges. Similar results for the critical Mach number have also been determined by Ogana[37] who divided the region of integration into a large number of rectangles and evaluated the integral by quadrature at each step of an iteration process.

Corresponding results for a NACA 0012 airfoil are presented in Fig. 7 together with an essentially

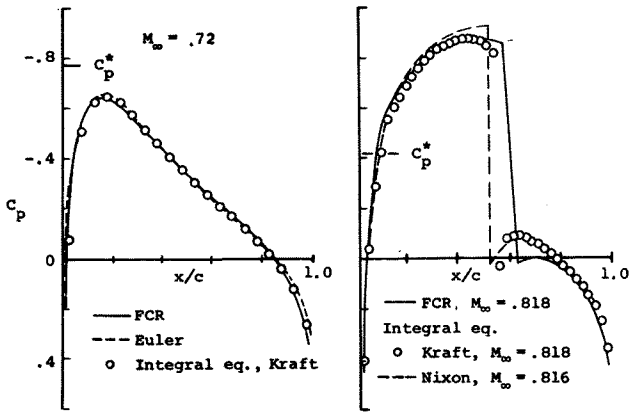

Fig. 7.- Pressure distributions for an NACA 0012 airfoil indicated by integral equation and FCR solutions of the transonic small disturbance equations, and by a numerical solution of the Euler equations.

exact solution of the Euler Eqs. (4)(52) for the subcritical case. The $x^{-1/2}$ singularity in u_L that would be present if the usual thin-airfoil boundary condition Eq. (8) were employed has been avoided in the integral equation results of Fig. 7 by using Eq. (14) for the boundary condition. Aside from modest differences near the shock, the integral equation results are virtually identical to those of the finite difference relaxation method and obtained with considerably less computation.

Attention is turned now to unsteady flow. Fig. 8 presents pressure distributions for an NACA 64A410 airfoil oscillating in pitch about a mean angle of attack of 2° in a flow with

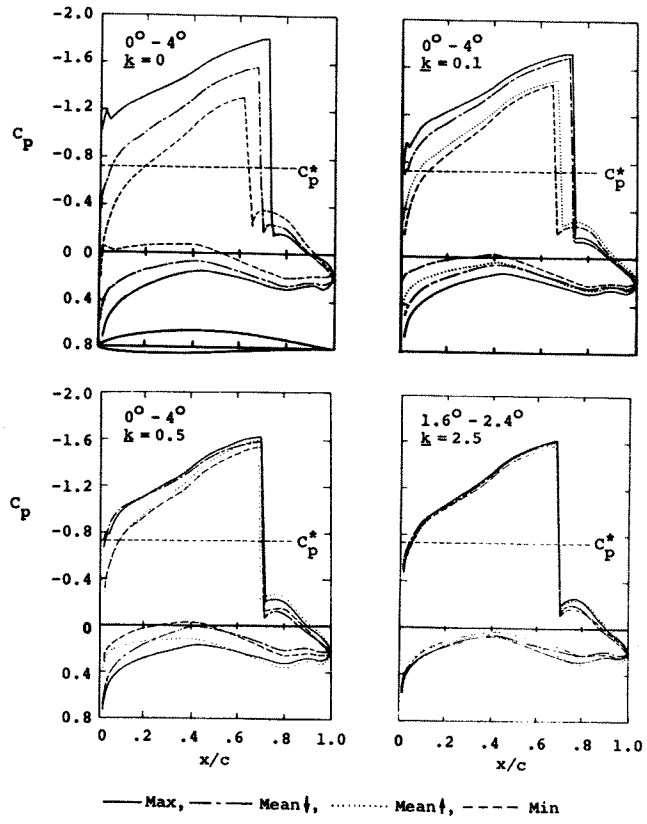

Fig. 8.- Time-dependent solution of Euler Eq. (5) for the pressure distribution on an NACA 64A410 airfoil oscillating in pitch.

$M_\infty = 0.72$, as calculated by Magnus and Yoshihara (21) using a time-dependent method to solve the Euler Eqs. (3). For the three smallest reduced frequencies $k = \omega c/2U_\infty$, the amplitude is 2°; but it is only 0.4° for $k = 2.5$. For each frequency, the pressure distributions on the upper and lower surfaces are shown for the minimum and maximum angles, and for the angle of attack both increasing and decreasing through the mean. At even the smallest frequency, $k = 0.1$, the results differ distinctly from those of quasi-stationary theory ($k = 0$). As k increases, the amplitude of the pressure variations diminishes, and the shock movement virtually vanishes for $k = 2.5$. The latter may be of importance to those developing approximate theories, since it suggests that shock movement may be disregarded for high frequency oscillations.

The results just described are of great theoretical significance; however, their computing cost is too high for the engineering analysis of aeroelastic and flutter problems which requires a large number of cases to be considered individually since solutions cannot be superposed. Simplification may be achieved by turning to the small disturbance theory for unsteady transonic flow, but the need to consider every case separately remains since Eq.(7) is nonlinear. For many applications, it is fruitful to decompose the problem into steady and unsteady components by letting

$$\phi = \bar{\phi} + \tilde{\phi}, \quad Z = \bar{Z} + \tilde{Z}, \quad C_p = \bar{C}_p + \tilde{C}_p \tag{15}$$

where the barred quantities satisfy Eqs. (7) through (9) with the time derivatives omitted. The remaining unsteady quantities should satisfy

$$(1 - M_\infty^2)\tilde{\phi}_{xx} - k(\bar{\phi}_x\tilde{\phi}_{xx} + \bar{\phi}_{xx}\tilde{\phi}_x + \tilde{\phi}_x\tilde{\phi}_{xx}) + \tilde{\phi}_{zz} - \frac{2M_\infty^2}{U_\infty}\tilde{\phi}_{xt} - \frac{M_\infty^2}{U_\infty^2}\tilde{\phi}_{tt} = 0 \tag{16}$$

for the boundary conditions and pressure relation given by Eqs. (8) and (9) with tildes over ϕ, Z, and C_p, but significant simplification can be achieved for small amplitude motions of an airfoil with nonvanishing steady-state disturbance field by disregarding $\tilde{\phi}_x\tilde{\phi}_{xx}$ to obtain a linear differential equation for $\tilde{\phi}$. Although the dependence of the variable coefficients $\bar{\phi}_x$ and $\bar{\phi}_{xx}$ on the nonlinear steady-state solution makes the equations more difficult to solve than those of ordinary linearized theory, $\tilde{C}_p$ is linearly dependent on the amplitude of the unsteady motion, and results for various unsteady motions about a single steady-state condition can be superposed to determine solutions for more complicated motions.

Fig. 9 presents results calculated in this way by Ehlers(53) using a finite difference relaxation method for an NACA 64A006 airfoil at zero angle of attack with an oscillating flap extending over the rear quarter chord. The results are qualitatively similar to the experimental data(54), but the unsteady pressures are generally overpredicted. Traci(55) et al., have confirmed Ehler's results by application of essentially the same method to the low frequency counterpart of Eq. (16) in which ϕ_{tt} is omitted in addition to the nonlinear term. Perhaps the most notable feature of the results is the unsteady pressure peak at about midchord in the supercritical example with $M_\infty = 0.853$ that is completely unheralded in the results for the subcritical example with $M_\infty = 0.794$. The peak at three-quarter chord is that normally expected at the hinge line for any subsonic flow. The second peak in the supercritical case is associated with the accumulation of receding waves as they move upstream from the flap until they are slowed and extensively refracted by the zone of supersonic flow. The data for $M_\infty = 0.90$ and 0.96 indicate that such effects disappear as expected when the flow upstream of the hinge line becomes supersonic.

Supplementing the development described above is a search for more economical approximate methods. Notable among these is an extension(56,57) of the local linearization method developed originally(39)

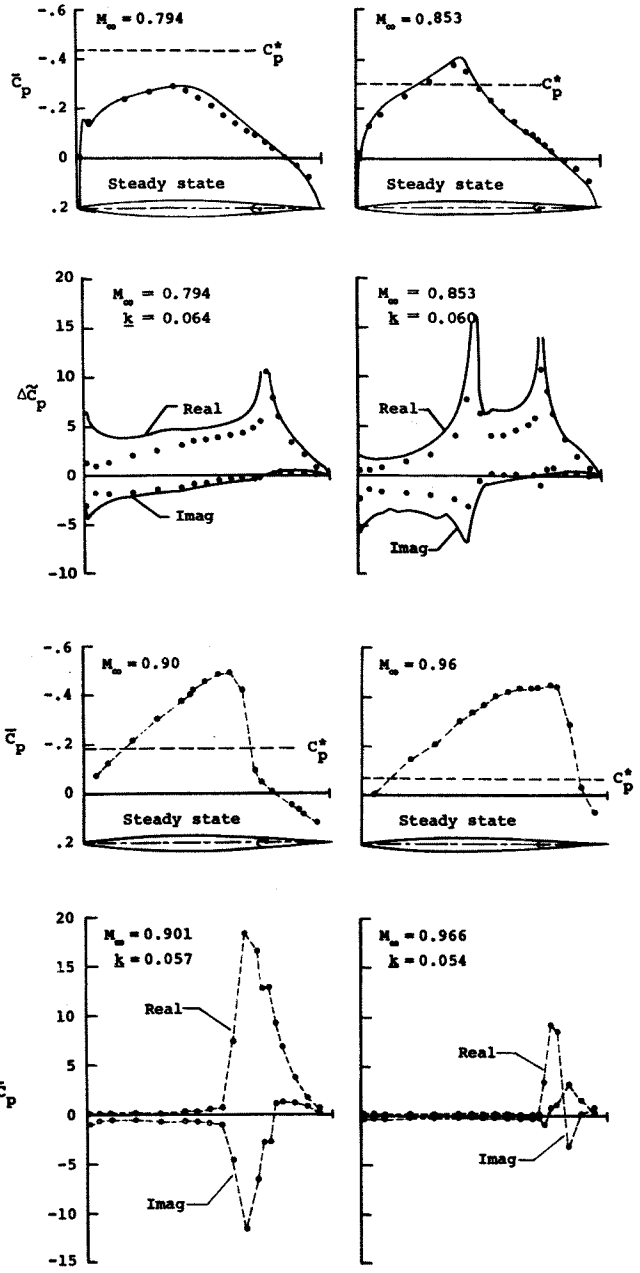

Fig. 9.- Pressure distributions on an NACA 64A006 airfoil with oscillating flap.

for steady flow. Results for the magnitude, $|\Delta\tilde{C}_p|$, and phase, $\Phi_{\tilde{C}_p}$, of the unsteady aerodynamic loading at $M_\infty = 1$ on a 6-percent thick circular-arc airfoil oscillating in pitch about the nose with ampltidue δ and various reduced frequencies $\underline{k}$ are shown in Fig. 10. Also included are the results of quasi-stationary theory and linearized theory to which the local linearization results converge for small and large $\underline{k}$. Rather similar results have been obtained by Isogai[58], Kimble and Wu[59], and Dowell[60] through application of somewhat different approximations based on the general notions of the local linearization method.

III. Axisymmetric and Related Slender-Body Flows

Several of the methods developed originally for two-dimensional flow have been extended to

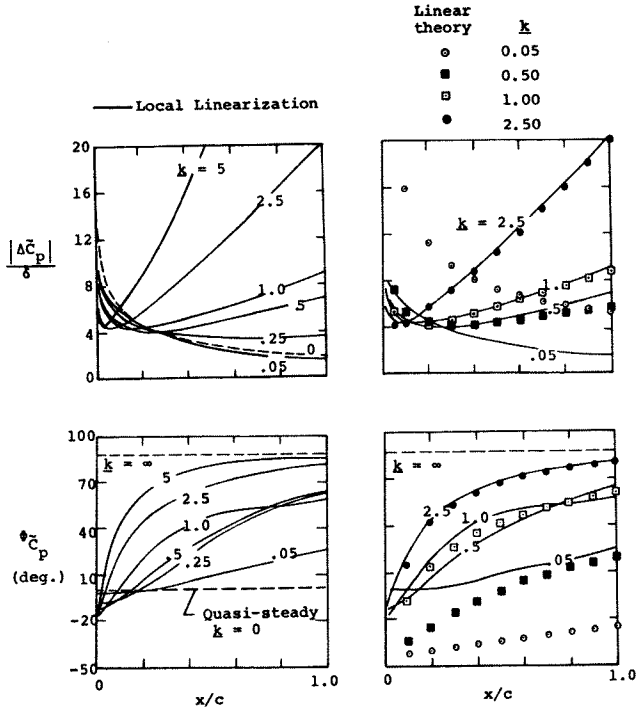

Fig. 10.- Load distribution on a thin circular-arc airfoil oscillating in pitch about the nose.

axisymmetric flow. Although some of the analyses have been based on the more complete theories, extensions to nonaxisymmetric slender bodies and wings have been confined almost exclusively to the small disturbance theory described by

$$(1 - M_\infty^2 - k\phi_x)\phi_{xx} + \phi_{yy} + \phi_{zz} - \frac{2M_\infty^2}{U_\infty}\phi_{xt} - \frac{M_\infty^2}{U_\infty}\phi_{tt} = 0 \quad (17)$$

together with appropriate boundary conditions, and a pressure relation modified to include $\phi_y^2 + \phi_z^2$ within the parentheses of Eq. (9).

Figure 11 shows pressure distributions for a 10-percent thick parabolic-arc body of revolution for several M_∞ from 0.9 to 1.1 calculated using the local linearization[61] and numerical NCR[62] methods together with experimental data[63]. These results, and also the previously unpublished FCR results calculated at NEAR, are in good agreement

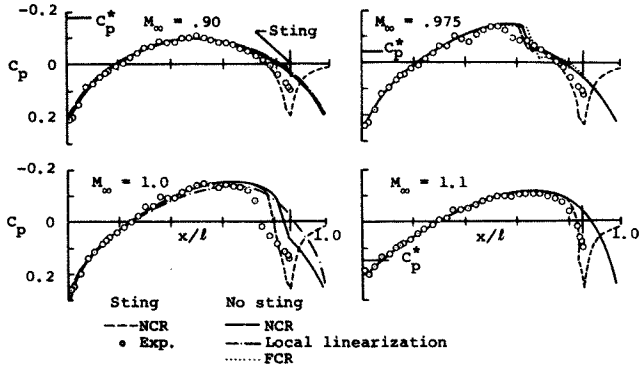

Fig. 11.- Pressure distributions for a parabolic-arc body of revolution indicated by various solutions of the small disturbance equations, and by experiment.

over most of the body, but notable differences exist near the rear. Some of these may be attributed to viscous phenomena, but effects of the cylindrical sting model support and wind tunnel walls are also significant. To demonstrate the effects of the sting, NCR results[62] are presented for a shape that conforms to the test model and sting combination. The results are in improved agreement with the data, but significant differences remain.

To investigate the effects of the walls, Bailey [62] carried out NCR calculations for the body-sting combination in a circular wind tunnel having the same cross-section area relative to the body as the Ames 14-foot wind tunnel where the tests were conducted. To simulate the ventilated walls of the test section, calculations were performed for a porous wall with various porosities. The results for a porosity of 0.5 are shown in Fig. 12 together with those for free air and for an open

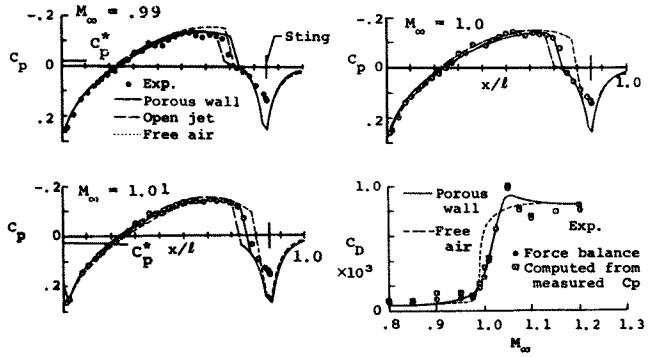

Fig. 12.- Pressure distributions and surface pressure drag for a parabolic-arc body of revolution with sting in free air, an open jet, and a wind tunnel with porous walls.

jet. Sedin and Karlsson[64] have obtained similar results for the porous wall using their alternating direction integration method. The theory indicates that the walls produce an upstream shift of the shock wave, thereby bringing the calculated pressure distribution and pressure drag into virtually perfect agreement with the measurements. Prudence should be exercised in accepting these results as definitive, however, since the boundary condition applied at the wall is a highly simplified representation of a complex local flow.

It has long been known[3] that the solution for certain thickness-dominated steady transonic flows past slender wings, bodies, and wing-body combinations can be decomposed into four simpler components by use of the transonic equivalence rule. As illustrated by Fig. 13 with ϕ_{xt} and $f(y,z;x,t)$ set to zero, three of these require solution of only the two-dimensional Laplace equation for flows in each transverse y,z plane; and the fourth requires solution of the transonic small disturbance equation for axisymmetric flow past an "equivalent" body of revolution having the same longitudinal distribution of cross-section area as the original aerodynamic shape. Cheng and Hafez[65] and Barnwell[66] have extended that result to lift-dominated cases, for which it is necessary to include additional higher-order (multipole) inner solutions beyond the first-order thickness (source) and lift (dipole) solutions.

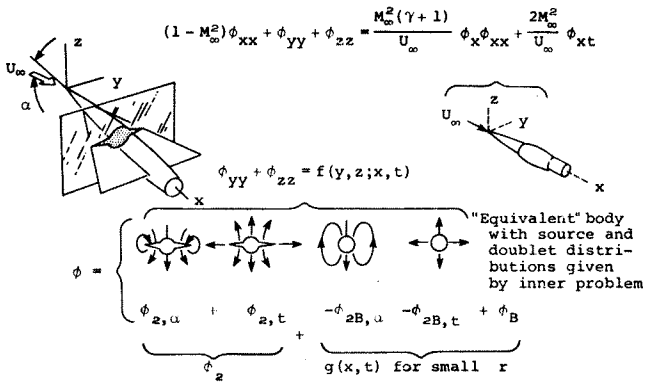

Fig. 13.- Schematic representation of unsteady transonic equivalence rule for slender wing-body combinations for mildly unsteady motions.

The first-order thickness and lift inner solutions satisfy the two-dimensional Laplace equation; but the higher-order solutions satisfy Poisson's equation in which the right-hand side $f(y,z;x)$ is a function of the lower-order solutions. We have recently extended the analysis to unsteady flows[57], arriving at the result portrayed in Fig. 13.

Figure 14 presents results of an application of the equivalence rule for steady flow with $M_\infty = 1$ to slender bodies with elliptic cross sections and the same longitudinal distribution of cross-section area as a parabolic-arc body of revolution of thickness ratio, 1/12[67]. The solution for the equivalent body was determined using the local

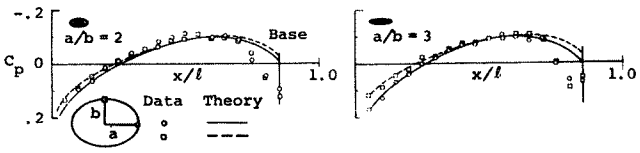

Fig. 14.- Pressure distributions on two parabolic-arc bodies of elliptic cross section; $M_\infty = 1$.

linearization method, the only method available at the time these results were originally published, and are for free-air flow past a complete body, i.e., without a sting. After making allowances for deficiencies over the rear of the body that can be attributed to effects of wind tunnel walls and model support, the results show that the equivalence rule provides a simple and accurate means for treating transonic flow past slender bodies of noncircular cross section.

Figure 15 presents a similar comparison of theoretical and experimental results for $M_\infty = 1$ for one of the elliptic cross-section bodies of Fig. 14 at angles of attack of 2°, 4°, and 6°[67]. Good agreement is again found along most of the body, with notable differences occurring on the rear. The latter could be rectified by replacing the solution for the equivalent body by a solution like that of Fig. 12 that accounts for effects of the model support and wind-tunnel walls.

In contrast to the foregoing, the development of methods for solving the nonlinear equations for unsteady axisymmetric and three-dimensional transonic flows has barely begun. We have applied the

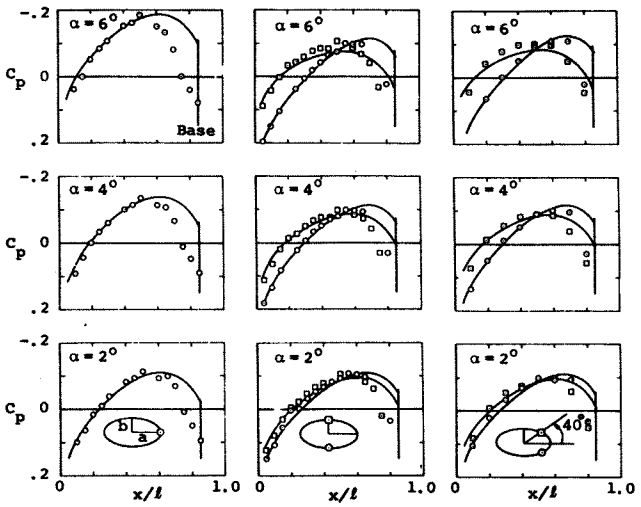

Fig. 15.- Pressure distributions on the body of Fig. 14 with $a/b = 2$ at three angles of attack, α; $M_\infty = 1$.

local linearization method to flow with $M_\infty = 1$ past a slender body of revolution engaged in a variety of unsteady motions. Fig. 16 reproduces results[57,68] for the amplitude and phase of the surface pressures on a nonlifting body undergoing

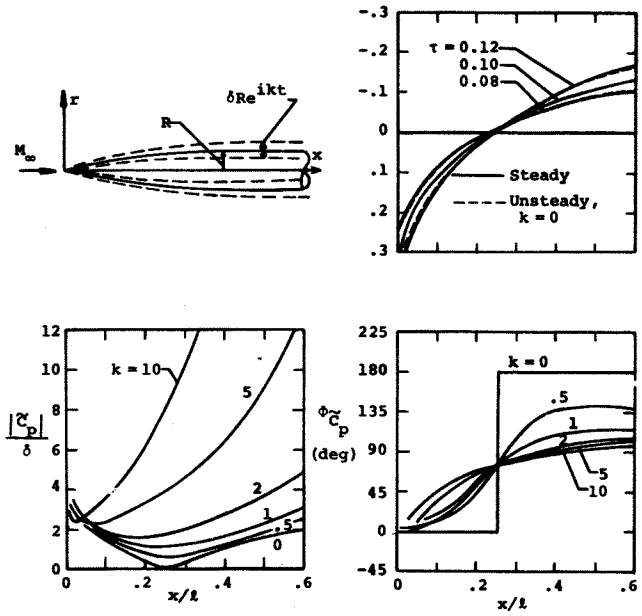

Fig. 16.- Local linearization solution for pressures on the forepart of a parabolic-arc body of revolution in oscillatory dilatation proportional to the local body radius; $\tau = 0.10$, $M_\infty = 1$.

small oscillatory dilatations proportional to the local body radius. As in the two-dimensional applications, the results approach those of linearized theory for high frequency oscillations, and quasi-stationary theory for low frequencies. The latter is illustrated in the plot in the upper right in which the pressure distributions indicated by the unsteady analysis for a basic body of thickness ratio, $\tau = 0.10$, undergoing slow expansion to $\tau = 0.12$ and contraction to $\tau = 0.08$ are shown to agree with local linearization solutions for steady flow past three such bodies. Extension of the local linearization analysis to the pitching motion of slender bodies of revolution at $M_\infty = 1$ has been carried out recently[69] and used to determine unsteady surface pressures and static and dynamic stability derivatives for conical and parabolic-arc bodies. The results are presented together with those of other approximate theories and are shown to agree well with available data.

IV. Three-Dimensional Flows Past Wings and Wing-Body Combinations

Much can be learned by the study of two-dimensional and slender-body flows, but rational aircraft design requires solutions for three-dimensional aerodynamic configurations. Fortunately, the finite difference relaxation method can be generalized to these situations, and modern computers are able to perform the computations in an acceptable time for steady flows past certain classes of three-dimensional shapes. To date, the analysis has been based almost exclusively on the small disturbance theory, which in its simplest form is described by Eq. 17 with ϕ_{xt} and ϕ_{tt} omitted.

Figures 17 and 18 present comparisons of calculated and experimental data for a swept ONERA M6 wing at an angle of attack of 3° for $M_\infty = 0.84$

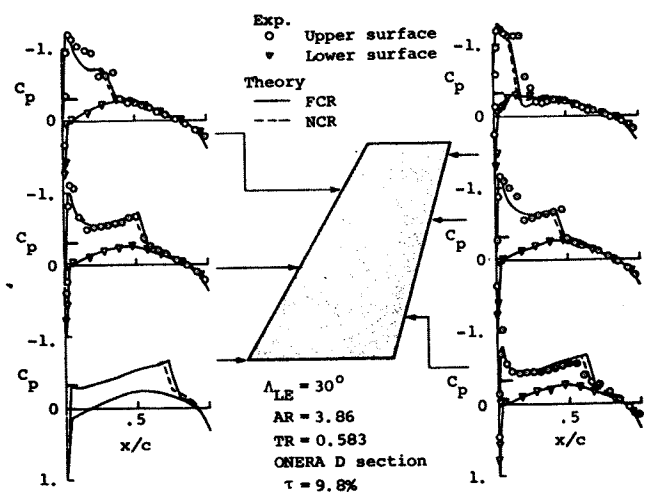

Fig. 17.- Pressure distributions on a swept ONERA M6 wing; $M_\infty = 0.84$, $\alpha = 3°$.

and 0.93[70]. Computations were performed using both the NCR and FCR methods and required about 5 CPU minutes on the CDC 7600 computer. As in the two-dimensional applications, the FCR method predicts a more downstream location for the shock wave than the NCR method, with the difference being more marked at the higher Mach number. Again, the data agree better with the NCR calculations, but this is certainly due to a fortuitous cancellation of errors in the shock jumps by disregarded viscous effects.

The experimental data also reveal a weak oblique shock upstream of the main shock and swept back about 35°, but no indication of it is given by the calculations. This is to be expected because

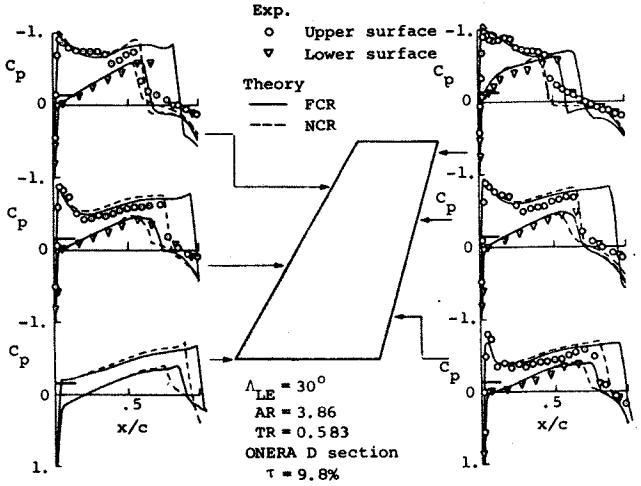

Fig. 18.- Pressure distributions on a swept ONERA M6 wing; $M_\infty = 0.93$, $\alpha = 3°$.

Eq. (17) provides a poor approximation for shocks with sweep angles greater than about 20°. A substantial improvement can be made, however, by adding two terms to Eq. (17) to obtain[10,71]

$$(1-M_\infty^2)\phi_{xx}+\phi_{yy}+\phi_{zz} = \frac{M_\infty^2(\gamma+1)}{U_\infty}\phi_x\phi_{xx} + \frac{M_\infty^2(\gamma-1)}{U_\infty}\phi_x\phi_{yy} + \frac{2M_\infty^2}{U_\infty}\phi_y\phi_{xy} \qquad (18)$$

for steady transonic flow. Studies of this and related extensions of the small disturbance theory are currently in progress. Moving closer to a complete airplane configuration, Fig. 19 presents experimental and NCR calculated pressures for a

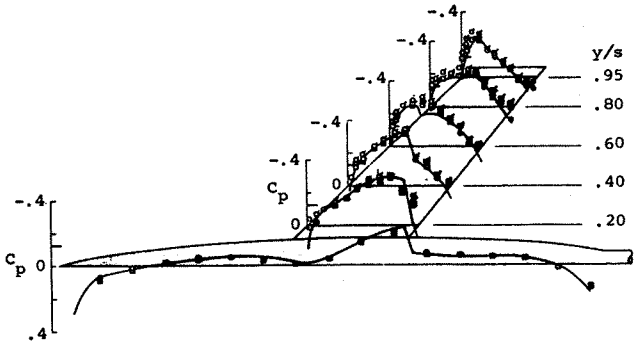

Fig. 19.- Pressure distribution on a wing-body combination; $M_\infty = 0.93$, $\alpha = 0°$.

swept-wing-fuselage configuration at $M_\infty = 0.93$ and $\alpha = 0°$[70]. The agreement with experiment is good along the fuselage centerline and the two inboard stations. In the computed results, the wing root shock propagates laterally to y/s = 0.60, but the experimental shock dissipates before reaching this point. The source of the disagreement is not clear but may be due to viscous effects or to deficiencies associated with swept shock waves.

As an alternative to the finite difference approach to three-dimensional transonic flow analysis, mention should be made of the alternating direction integration method of Sedin and Karlsson (64), which has recently been shown to be capable of providing plausible pressure distributions on wings and wing-body combinations. Further investigation of the accuracy and computational requirements of the method is necessary to determine its competitiveness with the finite difference methods.

V. Helicopter Rotors

The onset of transonic flow over the outer portion of the rotor blades is one of the primary conditions that sets the performance limits of modern helicopters. A transonic regime near a blade tip is inherently nonlinear, three-dimensional and, with forward flight, unsteady. As illustrated in Fig. 20[9], the shock on the upper surface moves downstream at points B and C, is nearly stationary at D, and moves upstream at E. Subsequently, the

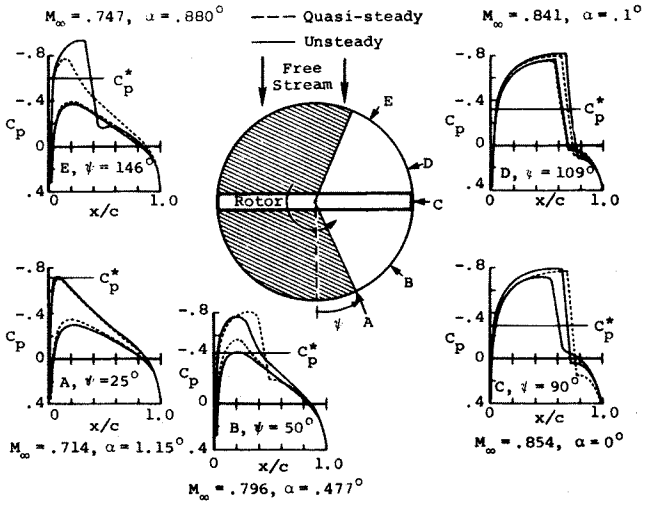

Fig. 20.- Pressure distributions for a simulated two-dimensional helicopter rotor.

shock propagates off the front of the airfoil into the oncoming flow. In the calculation of the theoretical results of Fig. 20, the unsteady motion of the rotor blade in forward flight was simulated by an NACA 0012 airfoil undergoing simultaneous sinusoidal Mach number and incidence variations with a phase difference of 180°. The governing equation is a two-dimensional low frequency version of Eq. (17) with ϕ_{yy} and ϕ_{tt} omitted and with $M_T + M_\infty \sin\psi$, which represents the instantaneous free-stream Mach number, in place of M_∞ in the coefficients of ϕ_{xt} and ϕ_{xx} and the boundary conditions. The quantity M_T is the tip Mach number due to rotation, and $\psi = \Omega t$ is the indicated azimuth angle on the rotor disk. The quasi-steady results were computed by solving the same equation with $\phi_{xt} = 0$, so that time appeared only as a parameter. The shaded region indicates the portion of the cycle for which the flow is subcritical, and for which the unsteady values for the pressures are nearly quasi-steady. In the supercritical region, however, the pressures and shock wave location lag the quasi-steady results.

The results of Fig. 20 correspond to strip theory, but three-dimensional effects are obviously important for a helicopter rotor, particularly near the tip. Caradonna and Isom[72] have investigated this feature of rotor aerodynamics, and calculated unsteady FCR solutions reproduced in Fig. 21 for both two- and three-dimensional representations.

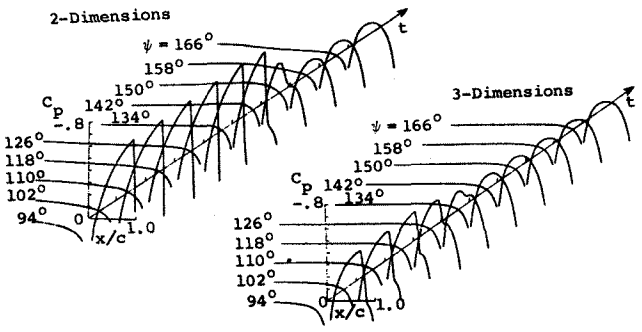

Fig. 21.- Two- and three-dimensional calculations of pressure distributions for several ψ at 97.7 percent of the rotor radius with blades of aspect ratio = 15 and 6-percent thick circular-arc profiles operating with an advance ratio, $U_\infty/\Omega R = 0.4$, and a tip Mach number, $M_T = 0.93$, at $\psi = 90°$.

Comparison shows that the three-dimensional solution indicates that the flow is far less expanded (the peak negative C_p is less in the supersonic region and the shock wave does not reach the trailing edge), the return to subsonic flow occurs earlier, and no upstream propagating wave is indicated for this case. Caradonna and Isom state that such a wave is seen in their results for a higher Mach number three-dimensional calculation, but its amplitude is about an order of magnitude less than indicated by the two-dimensional calculation. This brief account serves to indicate that helicopter aerodynamics provides a new field of application for transonic flow theory. The available results are very incomplete, but they illustrate the significance of transonic flow for helicopter rotors, and the need for a more comprehensive study.

VI. Rotating Turbomachinery

Flow through a high-speed fan or compressor is three dimensional, can include complex shock systems, and is unsteady even in a rotating frame of reference if a complete stage consisting of a rotor and stator or a fan preceded by inlet guide vanes is considered. Effects of viscosity and turbulence are important, particularly in the aft stages, and impact of the wake of one stage on the blades of the next is an important source of vibration and noise. The calculation of transonic flow through high-speed turbomachinery must be one of the most formidable problems in aerodynamics, but the technological need exists and methods are beginning to be developed.

In current work, the traditional approach is taken in which the inviscid flow field is considered first, leaving the viscous and turbulence effects to be added later, hopefully as small or localized perturbations. Since variations of pressure and flow direction may be substantial, the small disturbance theory is not expected to be as useful as it is for the external aerodynamics of the airplane. The appropriate equations for the inviscid analysis are, therefore, the Euler equations, or possibly the complete potential equation if the shock waves are not too strong. In the most advanced analysis, Erdos et al.,[73] have approximated the three-dimensional problem by a pair of two-dimensional problems, which are intended ultimately to be interacted to obtain the complete solution. Figure 22 presents the essential ideas of this decomposition and of the

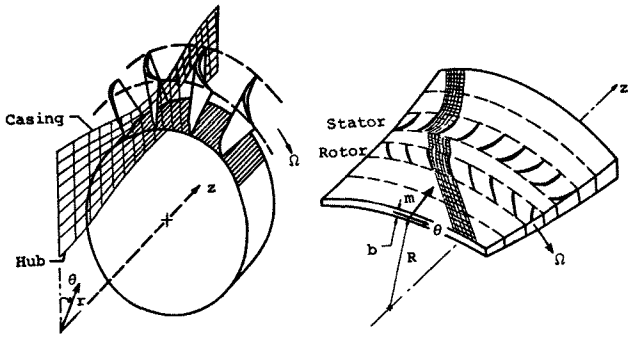

Fig. 22.- Coordinate systems and grid networks for interacting two-dimensional flows used to simulate three-dimensional flow through a rotor-stator stage of a turbomachine.

coordinate system evolved from it. The hub-to-casing solution accounts for effects of blockage of the flow area by the blades and the anticipated boundary layer as well as the geometry of the hub and casing, but not for any circumferential variations of the flow. It provides the flow properties in a meridional plane as averaged from one blade to the next, the coordinates $R = r(m)$ of the curved axisymmetric stream surface upon which the blade-to-blade analysis is carried out, and thereby the spacing $b(m)$ between two arbitrarily selected adjacent stream surfaces. The problem that must be solved for the blade-to-blade surface represents, therefore, a two-dimensional flow past a series of blades in the curvilinear coordinate system (m,θ) indicated in Fig. 22 with the radius, $R(m)$, and thickness, $b(m)$, of the stream sheet provided by the solution of the hub-to-casing solution. Expressed in a coordinate system rotating with the blades at an angular velocity Ω so as to obtain a steady flow problem if interaction with other blade rows is disregarded, the equations to be solved are

$$\frac{\partial \rho}{\partial t} + \frac{\partial(\rho V)}{R\partial\theta} + \frac{\partial(\rho U)}{\partial m} = -\frac{\rho U}{Rb}\frac{d(Rb)}{dm}$$

$$\frac{\partial(\rho V)}{\partial t} + \frac{\partial(p+\rho V^2)}{R\partial\theta} + \frac{\partial(\rho UV)}{\partial m} = -\frac{\rho UV}{Rb}\frac{d(Rb)}{dm} - \frac{\rho U}{R}(V+2\Omega R)\frac{dR}{dm}$$

$$\frac{\partial(\rho V)}{\partial t} + \frac{\partial(\rho UV)}{R\partial\theta} + \frac{\partial(p+\rho U^2)}{\partial m} = -\frac{\rho U^2}{Rb}\frac{d(Rb)}{dm} + \frac{\rho(V+\Omega R)^2}{R}\frac{dR}{dm}$$

$$\frac{\partial(\rho E_r)}{\partial t} + \frac{\partial(\rho V H_r)}{R\partial\theta} + \frac{\partial(\rho U H_r)}{\partial m} = -\frac{\rho U H_r}{Rb}\frac{d(Rb)}{dm} \qquad (19)$$

where U and V represent velocity components in the m and θ directions, and in which the relative total energy and total enthalpy are defined by

$$E_r = E - V\Omega R, \qquad H_r = H - V\Omega R \qquad (20)$$

The right-hand sides of Eq. (19), which differ from those of Erdos et al.(73) because of correction of errors in the transformation to curvilinear coordinates, arise from streamwise variations of thickness and radius of the stream sheet; they vanish if the equations are applied to a two-dimensional cascade flow. The corresponding equations for a nonrotating inertial system may be obtained by setting Ω to zero.

Only a few results obtained by solving these equations have been reported, and they are rather provisional because of the relatively small number of grid points used in the finite difference calculations. Results of blade-to-blade calculations of Erdos et al.,(73) are presented in Fig. 23 together with experimental data for a high-speed (1500-fps) fan tip section obtained

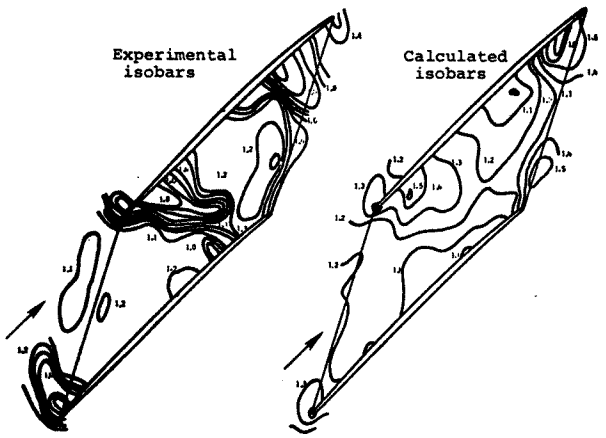

Fig. 23.- Experimental and calculated pressure distributions for flow through a 1500-fps rotor.

from an array of fast response pressure gages mounted on the casing wall. The test fan was preceded by a set of guide vanes and followed by a row of stators, but the unsteady interactions were neglected in the calculations and only the effects of the rotor was considered. Although the grid network was very coarse, the calculated flow bears a recognizable resemblance to the observations, particularly the indications of an oblique shock from the leading edge of the upper blade that reflects off the lower blade and reimpinges on the upper blade near the trailing edge. These developments give promise of substantial improvements in predictive capabilities for the design and analysis of high-speed turbomachinery. The flows are very complex, however, and continued effort will be required for some time before accurate and economical methods will be available for the routine solution of these problems.

VII. Concluding Remarks

The preceding discussion has provided a review of recent developments in steady and unsteady transonic aerodynamics. Many references are cited; but many significant contributions are not, or are hidden in references to summary papers. In many instances, the selection has been made on the basis of interlocking relations that help to evaluate the various results, and to provide a continuing base from which further discussion can proceed smoothly.

Overall, it is clear that tremendous advances are being made in the analysis of transonic flows, and that these problems no longer appear as formidable as they once did. Indeed, some of the simpler two-dimensional and axisymmetric steady flows may be considered solved, with even alternative methods available to choose among. The research frontier is moving now to more complex steady and unsteady three-dimensional flows past wings, wing-body combinations, helicopter rotors, and through turbomachinery fans and compressors. The modern computer has brought immense calculating power to bear on these problems, and the goal of replacing the wind tunnel with a computer is beginning to look more achievable than ever before. However, all will not fall into place by itself. Much work must be done, but the directions are indicated and the rewards of improved aerodynamic design and analysis are sufficient to demand the effort be made.

VIII. Acknowledgement

Acknowledgement is made for the support of this work to the Office of Naval Research under Contract N00014-73-C-0379/NR 061-215.

IX. References

1. von Kármán, T., "The Similarity Law of Transonic Flow," J. Math. & Phys., 16, 182-190, 1947.

2. Guderley, K. G., Theorie schallnaher Strömungen, Springer, 1957. Available in transl. (by J.R. Moszynski) as The Theory of Transonic Flow, Addison-Wesley, 1962.

3. Spreiter, J. R., "Aerodynamics of Wings and Bodies at Transonic Speeds," J. Aero/Space Sci., 26, 465-487, 1959.

4. Ferrari, C., and Tricomi, F. G., Aerodinamica Transonica, Edizioni Cremonese, 1962. Available in transl. (by R.H. Cramer) as Transonic Aerodynamics, Academic Press, 1968.

5. Oswatitsch, K., (Ed.), Symposium Transsonicum, Springer, 1964.

6. Oswatitsch, K., and Rues, D., Symposium Transsonicum II, Springer, 1976.

7. Jameson, A., "Transonic Flow Calculations," von Kármán Institute Lecture Series on Computational Fluid Dynamics, 1976.

8. Murman, E. M., (Ed.), Transonic Aerodynamics, AIAA Prof. Study Series, 1975.

9. Ballhaus, W. F., "Some Recent Progress in Transonic Flow Computation," von Kármán Institute Lecture Series on Computational Fluid Dynamics, 1976.

10. Bailey, F. R., "On the Computation of Two- and Three-Dimensional Steady Transonic Flows by Relaxation Methods," von Kármán Institute Lecture Series on Progress in Numerical Fluid Dynamics, 1974.

11. Wu, J. M., and Moulden, T. H., "A Survey of Transonic Aerodynamics," AIAA Paper No. 76-326, 1976.

12. Diewert, G. S., "Numerical Simulation of High Reynolds Number Transonic Flow," AIAA Jour., 13, 1354-1359, 1975.

13. Diewert, G. S., "Computation of Separated Transonic Turbulent Flow," AIAA Jour., 14, 735-740, 1976.

14. Rizzi, A., "Transonic Solutions of the Euler Equations by the Finite Volume Method," Symposium Transsonicum II, (Ed., K. Oswatitsch and D. Rues), Springer, 1976.

15. Magnus, R., and Yoshihara, H., "Inviscid Transonic Flow over Airfoils," AIAA Jour., 8, 2157-2162, 1970.

16. Nieuwland, G. Y., "Transonic Potential Flow Around a Family of Quasi-Elliptical Aerofoil Sections," NLR TR 172, 1967.

17. Takanashi, S., "A Method of Obtaining Transonic Shock-Free Flow Around Lifting Aerofoils," Trans. Japan Soc. Aero. Space Sci., 16, 34- , 1973.

18. Boerstoel, J. W., "Review of the Application of Hodograph Theory to Transonic Aerofoil Design and Theoretical and Experimental Analysis of Shock-Free Aerofoils," Symposium Transsonicum II, (Ed., K. Oswatitsch and D. Rues), Springer, 1976.

19. Bauer, F., Garabedian, P., and Korn, D., Supercritical Wing Sections, Lecture Notes in Economics and Mathematical Systems, 66, Springer, 1972.

20. Bauer, F., Garabedian, P., Korn, D., and Jameson, A., Supercritical Wing Sections II, Lecture 108, Springer, 1975.

21. Magnus, R., and Yoshihara, H., "Finite Difference Calculations of the NACA 64A-410 Airfoil Oscillating Sinusoidally in Pitch at $M_\infty = 0.72$," Tech. Dept. CASD-NSC-74004, Convair Div. of Gen. Dyn., 1974.

22. Yoshihara, H., "A Survey of Computational Methods of 2D and 3D Transonic Flows with Shocks," GDCA-ERR-1726, Convair Aerospace Div. of Gen. Dyn., 1972. Also available in Transonic Aerodynamics, (Ed. E. M. Murman), AIAA Prof. Study Series, 1975.

23. Emmons, H. W., "Flow of a Compressible Fluid Past a Symmetrical Airfoil in a Wind Tunnel and in Free Air," NACA TN 1746, 1948.

24. Vincenti, W. G., and Wagoner, C. B., "Transonic Flow Past a Wedge Profile with Detached Bow Wave," NACA Rep. 1095, 1952.

25. Vincenti, W. G., Wagoner, C. B., and Fisher, N. H. Jr., "Calculations of the Flow Over an Inclined Flat Plate at Free Stream Mach Number One," NACA TN 3723, 1956.

26. Murman, E. M., and Cole, J. D., "Calculation of Plane Steady Transonic Flows," AIAA Jour., 9, 114-121, 1971.

27. Murman, E. M., "Analysis of Embedded Shock Waves Calculated by Relaxation Methods," AIAA Jour., 12, 626-633, 1974.

28. Jameson, A., "Iterative Solution of Transonic Flows Over Airfoils and Wings, Including Flows at Mach 1," Commun. Pure Appl. Math., 27, 283-309, 1974.

29. Martin, E. D., "A Fast Semidirect Method for Computing Transonic Aerodynamic Flows," Proc. AIAA 2nd Computational Fluid Dynamics Conf., 1975.

30. Ballhaus, W. F., and Steger, J. L., "Implicit Approximate-Factorization Schemes for the Low-Frequency Transonic Equation," NASA TM X-73,082, 1975.

31. Oswatitsch, K., "Die Geschwindigkeitsverteilung an symmetrischen Profilen beim Auftreten lokaler Überschallgebiete," Acta Physica Austriaca, 4, 228-271, 1950.

32. Spreiter, J. R., and Alksne, A. Y., "Theoretical Prediction of Pressure Distributions on Nonlifting Airfoils at High Subsonic Speeds," NACA Rep. 1217, 1955.

33. Nixon, D., and Hancock, G. J., "Integral Equation Methods - a Reappraisal," Symposium Transsonicum II, (Ed., K. Oswatitsch and D. Rues), Springer, 1976.

34. Ogana, W., and Spreiter, J. R., "Derivation of an Integral Equation for Transonic Flows," Submitted to AIAA Jour., 1975.

35. Spreiter, J. R., Alksne, A. Y., and Hyett, B. J., "Theoretical Pressure Distributions for Several Related Nonlifting Airfoils at High Subsonic Speeds," NACA TN 4148, 1958.

36. Kraft, E. M., "An Integral Equation Method for Boundary Interference in Perforated-Wall Wind Tunnels at Transonic Speeds," Ph.D. Dissertation, Univ. Tenn., 1975.

37. Ogana, W., "Computation of Steady Two-Dimensional Transonic Flows by an Integral Equation Method," Ph.D. Dissertation, Stanford Univ., 1975.

38. Spreiter, J. R., and Alksne, A. Y., "Thin Airfoil Theory Based on Approximate Solution of the Transonic Flow Equation," NACA Rep. 1359, 1958.

39. Spreiter, J. R., "The Local Linearization Method in Transonic Flow Theory," Symposium Transsonicum, (Ed., K. Oswatitsch), Springer, 1964.

40. Rubbert, P., and Landahl, M., "Solution of the Transonic Airfoil Problem Through Parametric Differentiation," AIAA Jour., 5, 470-479, 1967.

41. McDevitt, J. B., Levy, L. L., Jr., and Diewert, G. S., "Transonic Flow About a Thick Circular-Arc Airfoil," AIAA Jour., 14, 606-613, 1976.

42. Steger, J. L., and Lomax, H., "Transonic Flow About Two-Dimensional Airfoils by Relaxation Procedures," AIAA Jour., 10, 1972.

43. Garabedian, P. R., and Korn, D. G., "Analysis of Transonic Airfoils," Commun. Pure Appl. Math., 14, 841-851, 1973.

44. Lock, R. C., "Test Cases for Numerical Methods in Two-Dimensional Transonic Flows," AGARD Rept. NO1 575, 1970.

45. Krupp. J. A., and Murman, E. M., "The Numerical Calculation of Steady Transonic Flows Past Thin Lifting Airfoils and Slender Bodies," AIAA Paper No. 71-566, 1971.

46. Spreiter, J. R., "On the Application of Transonic Similarity Rules to Wings of Finite Span," NACA Rep. 1153, 1953.

47. Krupp, J. A., "The Numerical Calculation of Plane Steady Transonic Flows Past Thin Lifting Airfoils," Boeing Scientific Research Lab. Rep. D180-12958-1, 1971.

48. Knechtel, E. D., "Experimental Investigation at Transonic Speeds of Pressure Distributions over Wedge and Circular-Arc Airfoil Sections and Evaluations of Perforated-Wall Interference," NASA TN D-15, 1959.

49. Newman, P. A., and South, J. C., Jr., "Conservative Versus Nonconservative Differencing: Transonic Streamline Shape Effects," NASA TM X-72827, 1976.

50. Magnus, R. M., "The Direct Comparison of the Relaxation Method and the Pseudo-Unsteady Finite Difference Method for Calculating Steady Planar Transonic Flow," TN-73-SP03, Convair Aerospace Div. of Gen. Dyn., 1973.

51. Nixon, D., "Calculation of Transonic Flows Using an Extended Integral Equation Method," AIAA Paper No. 75-876, 1975.

52. Sells, C. C. L., "Plane Subcritical Flow Past a Lifting Airfoil," Proc. Roy. Soc., London, 308 (Series A), 377-401, 1968.

53. Ehlers, F. E., "A Finite Difference Method for the Solution of the Transonic Flow Around Harmonically Oscillating Wings," NASA CR-2257, 1975.

54. Tijdeman, H., and Schippers, P., "Results of Pressure Measurements of an Airfoil with Oscillating Flap in Two-Dimensional High Subsonic and Transonic Flow (Zero Incidence and Zero Mean Flap Position)," NLR TR 73078 U, 1973.

55. Traci, R. M., Albano, E. D., Farr, J. L., Jr., and Cheng, H. K., "Small Disturbance Transonic Flows About Oscillating Airfoils," AFFDL-TR-74-37, 1974.

56. Stahara, S. S., and Spreiter, J. R., "Development of a Nonlinear Unsteady Transonic Flow Theory," NASA CR-2258, 1973.

57. Spreiter, J. R., and Stahara, S. S., "Unsteady Transonic Aerodynamics - An Aeronautical Challenge," Unsteady Aerodynamics, (Ed., R. B. Kinney), Univ. Ar., 1975.

58. Isogai, K., "Unsteady Transonic Flow Over Oscillating Circular-Arc Airfoils," AIAA Paper No. 74-360, 1974.

59. Kimble, K. R., and Wu, J. M., "An Approximate Solution of Unsteady Transonic Flow Problems," AFFDL-TR-74-32, 1974.

60. Dowell, E. H., "A Simplified Theory of Oscillating Airfoils in Transonic Flow," Unsteady Aerodynamics, (Ed., R. B. Kinney), Univ. Ar., 1975.

61. Spreiter, J. R., and Alksne, A. Y., "Slender Body Theory Based on Approximate Solution of the Transonic Flow Equation," NASA Rep. R-2, 1959.

62. Bailey, F. R., "Numerical Calculation of Transonic Flow About Slender Bodies of Revolution," NASA TN D-6582, 1971.

63. Taylor, R. A., and McDevitt, J. B., "Pressure Distributions at Transonic Speeds for Parabolic-Arc Bodies of Revolution Having Fineness Ratios of 10, 12, and 14," NACA TN 4234, 1958.

64. Sedin, Y. c-J., and Karlsson, K. R., "Some Numerical Results of a New Three-Dimensional Transonic Flow Method," Symposium Transsonicum II, (Ed., K. Oswatitsch and D. Rues), Springer, 1975.

65. Cheng, H. K., and Hafez, M. M., "Transonic Equivalence Rule: A Nonlinear Problem Involving Lift," J. Fluid Mech., 72, 161-187, 1975.

66. Barnwell, R. W., "Transonic Flow About Lifting Configurations," AIAA Jour., 11, 764-766, 1973.

67. Spreiter, J. R., and Stahara, S. S., "Aerodynamics of Slender Bodies and Wing-Body Combinations at $M_\infty = 1$," AIAA Jour., 9, 1784-1791, 1971.

68. Stahara, S. S., and Spreiter, J. R., "Unsteady Local Linearization Solution for Dilatory Oscillation of Bodies of Revolution at $M_\infty = 1$," AIAA Jour., 14, 990-992, 1976.

69. Stahara, S. S., and Spreiter, J. R., "Unsteady Local Linearization Solution for Pitching Bodies of Revolution at $M_\infty = 1$: Stability Derivative Analysis," AIAA Jour. (in press).

70. Bailey, F. R., and Ballhaus, W. F., "Comparisons of Computed and Experimental Pressures for Transonic Flows About Isolated Wings and Wing-Fuselage Configurations," NASA SP-347, 1975.

71. Lock, R. C., "Research in the UK on Finite Difference Methods for Computing Steady Transonic Flows," Symposium Transsonicum II, (Ed., K. Oswatitsch and D. Rues), Springer, 1975.

72. Caradonna, F. X., and Isom, M. P., "Numerical Calculation of Unsteady Transonic Potential Flow over Helicopter Rotor Blades," AIAA Jour., 14, 482-488, 1976.

73. Erdos, J., Alzner, E., Kalben, P., McNally, W., and Slutsky, S., "Time-Dependent Transonic Flow Solutions for Axial Turbomachinery," NASA SP-347, 1975.